Remote Sensing Applications: Society and Environment 34 (2024) 101191

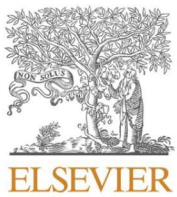

Contents lists available at ScienceDirect

Remote Sensing Applications: Society and Environment

journal homepage: www.elsevier.com/locate/rsase

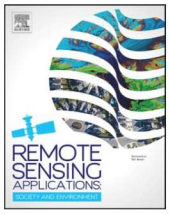

Ground deformation monitoring via PS-InSAR time series: An industrial zone in Sacco River Valley, central Italy

Ebrahim Ghaderpour [a,b,*], Paolo Mazzanti [a,b], Francesca Bozzano [a,b], Gabriele Scarascia Mugnozza [a,b]

[a] Department of Earth Sciences & CERI Research Centre, Sapienza University of Rome, P.le Aldo Moro, 5, Rome, 00185, Italy
[b] NHAZCA S.r.l., Via Vittorio Bachelet, 12, Rome, 00185, Italy

ARTICLE INFO

Keywords:
Climate change
Rainfall/runoff
Remote and satellite sensing
Sacco river valley
Subsidence
Turning point detection
Wavelet analysis

ABSTRACT

Persistent Scatterer Interferometric Synthetic Aperture Radar (PS-InSAR) is an advanced technique enabling effective ground deformation monitoring. In this study, PS-InSAR time series of Sentinel-1 ascending and descending orbits for period 2015–2022 are utilized for an industrial zone in Sacco River Valley, Central Italy. The Sequential Turning Point Detection (STPD) is applied to estimate the trend turning points and their directions in PS-InSAR time series. In addition, river flow and climate time series for Sacco River near the industrial zone are analyzed using the coefficient of determination and the Least-Squares Cross-Wavelet Analysis (LSCWA) to investigate their potential impact on ground deformation. A significant land subsidence was observed prior to Fall 2016 likely as the result of drought and excessive water extraction followed by land uplift after Fall 2017 likely due to groundwater rebound. The LSCWA showed statistically significant seasonal coherency between precipitation and streamflow in 2018 when relatively much higher precipitation and streamflow were observed in this year compared to 2016 and 2017, potentially contributing to the land uplift in the study zone during 2018. These results not only highlight the capabilities of STPD for detecting trend turning points and LSCWA for analyzing streamflow and precipitation time series but also can help policymakers and stakeholders for developing a sustainable city and environment.

1. Introduction

Ground deformation can modify the Earth surface physical parameters and cause severe damage to infrastructure, including railroads, buildings, pipelines, and others. In industrial zones, variations in groundwater level due to hydrocarbon extraction or aquifer overexploitation can result in land subsidence, especially during drought periods (Beccaro et al., 2019; Coda et al., 2019b). On the other hand, stopping overexploitation can result in groundwater rebound which can trigger land uplift, especially during relatively wetter periods (Allocca et al., 2022; Bai et al., 2016; Coda et al., 2019a; Colombo et al., 2017). For example, Tang et al. (2022) demonstrated how groundwater rebound of aquifer system in Taiyuan basin in northern China resulted in land uplift by analyzing Sentinel-1 satellites data. Jasechko et al. (2024) utilized groundwater level data for 1693 aquifer systems and 170,000 monitoring wells in many countries. They demonstrated that groundwater level has been declining more rapidly in 30% of regional aquifers across the world over the past four decades, and they also showed specific cases where groundwater level declining trend has been reversed

* Corresponding author. Department of Earth Sciences & CERI Research Centre, Sapienza University of Rome, P.le Aldo Moro, 5, Rome, 00185, Italy.
E-mail address: ebrahim.ghaderpour@uniroma1.it (E. Ghaderpour).

https://doi.org/10.1016/j.rsase.2024.101191
Received 6 December 2023; Received in revised form 12 February 2024; Accepted 18 March 2024
Available online 19 March 2024

following proper managements and policy changes. Therefore, it is crucial to continuously monitor ground deformation and develop a sustainable management plan to reduce the potential risks.

Interferometric SAR (InSAR) is a ground deformation mapping technique that uses radar images of the Earth surface acquired from orbiting satellites (Hu et al., 2018; Moretto et al., 2021; Rosen et al., 2000). Differential InSAR (DInSAR) is another technique that can observe phase changes between two images in each time and has been utilized in various studies for ground deformation monitoring (Calò et al., 2014; Crosetto et al., 2016; Mazzanti et al., 2015; Rocca et al., 2014). However, interferograms often contain wide areas where the signals decorrelate, and it is not possible to acquire measurements (Sousa et al., 2010). Bozzano et al. (2015) utilized the Advanced DInSAR technique to investigate the land subsidence in Acque Albule Plain in the east of Rome, central Italy for period 1993–2010. They showed that the groundwater level fluctuations triggered the land subsidence, and the magnitude of deformation depended on the thickness of the compressible deposits in their study area.

Persistent Scatterer InSAR (PS-InSAR) is an advanced technique which determines resolution elements such that their echo is highly significant by a single scatterer in a series of interferograms, overcoming the decorrelation problem in DInSAR technique (Crosetto et al., 2016; Sousa et al., 2010). Ascending and descending PS-InSAR time series are employed in many studies for ground deformation monitoring, such as land subsidence by ground water extraction in urban areas and landslide monitoring (Hussain et al., 2022; Mateos et al., 2017; Yao et al., 2022). The Sentinel-1 satellites revisit the same geographic location along both ascending (from the south pole to the north pole) and descending (from the north pole to the south pole) orbits. Therefore, ascending and descending data are acquired over the same location in different times, allowing an effective estimation of the vertical and east-west components of displacement (Ren et al., 2022). Though PS-InSAR time series are unevenly sampled and contain seasonal noise due to atmospheric noise and phase unwrapping issues, their cumulative deformation and velocity are very good (Yao et al., 2022; Zhang et al., 2011). The European Ground Motion Service (EGMS) has recently provided Sentinel-1 PS-InSAR time series that are already pre-processed and publicly available, spanning 2015–2021 (7 years).

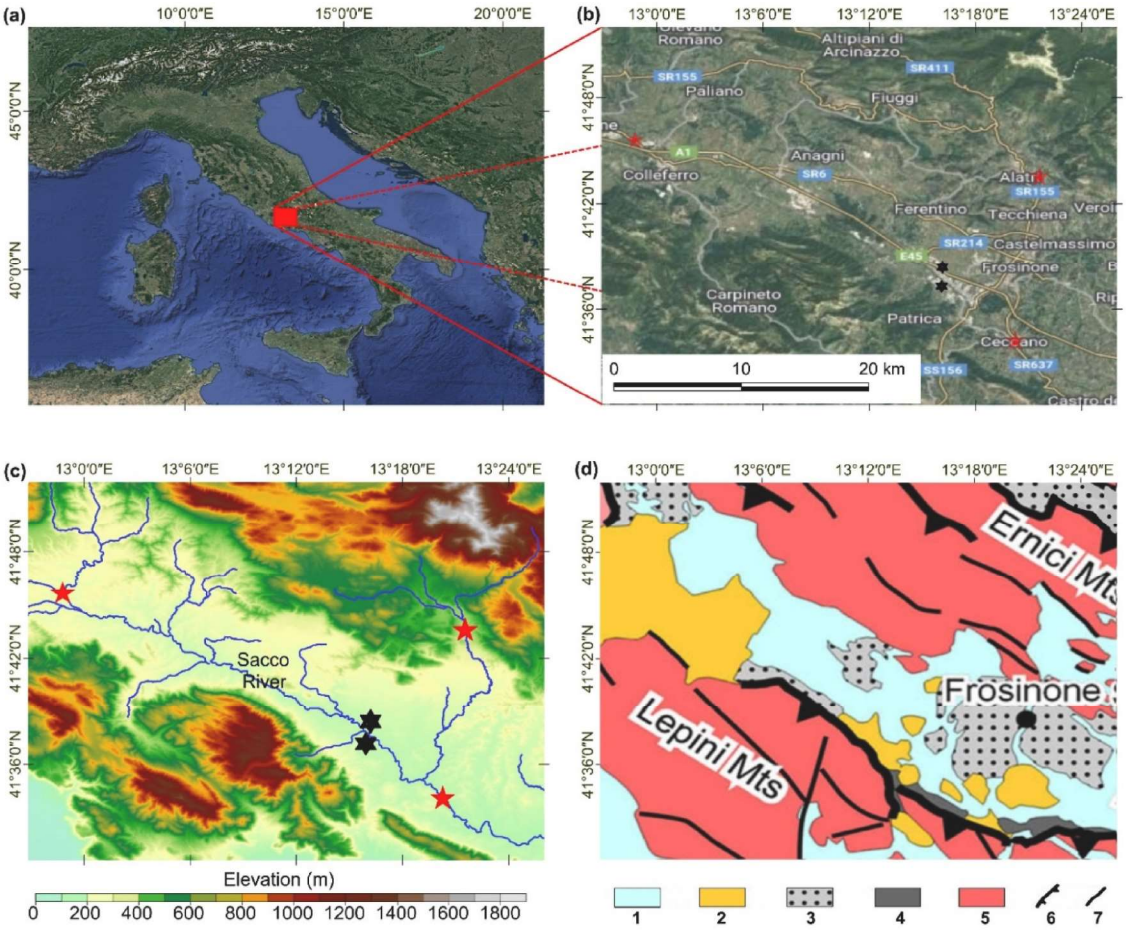

Fig. 1. (a) Google map of Italy showing the study region inside the red box, (b) Google hybrid map showing the hydrometric and weather stations along with the locations of two PS-InSAR as an example of ground deformation, (c) A 10 m resolution Digital Elevation Model (DEM) of the study region with an overlaid river network, and (d) Geological/hydrogeological structural map of Sacco River Valley (SRV), a section of the map shown by Saroli et al. (2019), where the numbers in the legend correspond to (1) Plio-Quaternary marine to continental clastic deposit (Pliocene–Holocene); (2) Quaternary volcanic deposit (Middle Pleistocene–Upper Pleistocene); (3) Messinian to Tortonian foredeep clayey sequence; (4) Miocene to Oligocene clayey units of the Molise-Sannio basin (Sicilidi Auct.); (5) Miocene to Trias shallow water carbonate sequence; (6) main thrust fronts; and (7) normal and/or strike-slip faults. (For interpretation of the references to color in this figure legend, the reader is referred to the Web version of this article.)

In literature, there are many Change-Point (CP) detection methods for time series, proposed for various purposes, including environmental monitoring (Awty-Carroll et al., 2019; Ghaderpour et al., 2021a). A CP in a time series is a date when there is an abrupt change (jump) or when the linear trend changes its gradient (turning point), or a phenological change (Li et al., 2022). The Sequential Turning Point Detection (STPD) is a fast and robust method of detecting turning points (Ghaderpour et al., 2024). A turning point (TP) in PS-InSAR displacement time series may be caused by slow-moving landslides, land subsidence or uplift. Enforcing the condition of no jumps, i.e., connected linear trend pieces, Ghaderpour et al. (2024) showed that STPD can estimate the location of TPs more accurately and faster than other CP detection methods, such as Pettitt and Running Slope Difference. Note that a TP is always a CP, but a CP may be an abrupt change or sudden jump that is not a TP. Therefore, one of the applications of STPD is detecting the dates when land started to subside or uplift (vertical displacement) through processing of PS-InSAR time series. Hereafter, a TP corresponds to a date when the gradient of linear trend in a time series changes significantly (in case of connected linear pieces only). The direction of a TP in a time series is the gradient of the linear trend piece after the TP (and before the next TP if any) minus the gradient of the linear trend piece before the TP (and after the previous TP if any).

Climate change and anthropogenic activities can significantly affect surface water and groundwater levels (Wuetal., 2020; Zaghloul et al., 2022). High temperature increases evaporation which can limit the water amount to recharge groundwater. On the other hand, anthropogenic influence on groundwater is due to excessive water pumping that can potentially cause land to subside (Li et al., 2021; Teatini et al., 2005; Wu et al., 2020). Many researchers studied the impact of groundwater variation and climate change on land subsidence and uplift through machine learning models, such as random forest (Chen et al., 2020; Fu et al., 2023). The quantitative interaction between groundwater and surface water is a challenging task (Jiang et al., 2022; Wang et al., 2023). Groundwater can be recharged by surface water in flooding seasons while groundwater can contribute to surface water in dry periods (Saha et al., 2017). In the present study, since groundwater data were not available, the surface water (river discharge) and climate data were utilized as an alternative solution. The main contributions of this study are.

- Mapping dates when the velocity of ground displacement changes (mapping TPs) and mapping the directions of TPs in an industrial zone in Sacco River Valley (SRV) in Central Italy using ascending and descending PS-InSAR time series. Also, mapping the overall velocities of ground motion toward satellite line-of-sight and reprojected vertical and east-west directions.
- Analyzing meteorological and streamflow time series around the industrial zone using the coefficient of determination and wavelet analyses.
- Discussing how climate and streamflow variations may have triggered the observed ground deformation in the industrial zone.

The rest of this article is organized as follows. Section 2 briefly describes the study region and employed datasets, as well as a brief description of the utilized data analytics methods. Section 3 demonstrates the geospatial maps of ground deformation as well as the meteorological and streamflow results. Section 4 discusses the potential causes of the ground deformation in the study region, and finally Section 5 concludes this article.

2. Materials and methods

2.1. Study region

The study region includes an industrial zone located between towns of Colleferro and Ceccano in the province of Frosinone in Lazio, central Italy, see Fig. 1. The Sacco River passes through this zone with an average discharge of 16 m^3/s. This river is formed by the confluence of two streams of the Monti Simbruini in the Apennines of Abruzzo in Lazio and has a total length of 87 km which flows into the Liri River from the right. There are numerous industrial settlements along the Sacco River (Massimo et al., 2014). The annual average precipitation of the study region is about 1600 mm estimated from the precipitation record from 2015 to 2022 (7 years). The annual average minimum and maximum temperatures of the region in that period are also 10 °C and 20 °C, respectively. In addition, the topographic slope in the industrial zone is less than 5°, Fig. 1(c).

Sacco River Valley (a part of Latina Valley), a vast territory between the provinces of Rome and Frosinone, has been mainly formed by lava flows from volcanoes (Saroli et al., 2020). The Quaternary deposits thickness in this region has been influenced by inherited paleo-morphologies, Fig. 1(d). The groundwater surface depth in SRV is approximately between 5 and 15 m, and its closeness to topsoil has favored water wells and aquifers pollution. A high amount of precipitation, particularly during fall and winter, and presence of flat

Table 1
Datasets utilized in this study and their brief descriptions. The discharge time series record for *Cosa ad Alatri* was available until 2020.

Dataset	Spatial Resolution	Date	Description	Source/Reference
DEM	10 m	2023	TINITALY	Tarquini and Nannipieri (2017), Tarquini et al. (2023)
PS-InSAR	20 m in azimuth by 5 m in ground-range	February 2015–December 2021 (6-day)	Ascending and Descending PS-InSAR Time Series	https://egms.land.copernicus.eu/ EGMS – Basic Products (Level 2)
PS-InSAR	100 m	January 2016–December 2021 (6-day)	Vertical and East-West PS-InSAR	https://egms.land.copernicus.eu/ EGMS– Ortho Products (Level 3)
Precipitation and Temperature	3 Weather Stations	January 2015–December 2021 (Monthly)	For Colleferro, Alatri, and Ceccano	https://www.3bmeteo.com
Discharge	3 Hydrometric Stations	January 2015–December 2021 (Monthly)	For Colleferro, Alatri, and Ceccano	https://temporeale.regione.lazio.it/aegis/map/map2d

areas, high permeability of karst rocks, and quaternary volcanic deposits significantly contribute to groundwater recharge processes in central-southern parts of Italy, including SRV (Allocca et al., 2015). Karst aquifers are the main source of drinking water supplies in the study region and have a high impact on other groundwater dependent ecosystems (Allocca et al., 2014). Due to improper management, SRV has been heavily polluted by industrial waste over the years which led to unprecedented environmental and health issues (Perrone et al., 2022). The SRV is one of the Italian contaminated sites of national interest (https://www.isprambiente.gov.it/).

2.2. Datasets and preprocessing

The descriptions of the datasets utilized in this work are listed in Table 1. The ascending and descending PS-InSAR time series, the EGMS basic products (Level 2), available from 2015 to 2022 are downloaded from the EGMS website. The EGMS basic products provide InSAR displacement measurements in the direction of satellite line-of-sight and are spatially referenced to a virtual reference point which are meaningful just for the processed area, see the EGMS product guide available online at https://land.copernicus.eu/. The sampling frequency of these time series is 6-day with many missing values. To perform STPD, the PS-InSAR time series are monthly resampled using the MATLAB spline interpolation code. Since there was at least one displacement measurement for each month from 2015 to 2022, the monthly resampled time series nicely captured the overall fluctuation of the displacement time series while attenuating noise. The EGMS Ortho products (Level 3), available from 2016 to 2022, are also employed herein to map the overall velocities of vertical and east-west ground motion for the industrial zone. These products contain vertical and east-west displacement components at spatial resolution of 100 m, derived by combining all the ascending and descending time series and considering the information of GNSS (Global Navigation Satellite Systems) measurements (Notti et al., 2014; Festa et al., 2022).

The monthly average discharge, minimum and maximum temperatures, and accumulated precipitation were also calculated from the downloaded datasets. Thus, for comparison purposes, all the datasets employed in this study are monthly resampled. The monthly scale is chosen herein for visualization purposes which is also robust for monitoring slow-moving ground deformation and climate studies. The names of hydrometric gauging stations with available discharge record within the study region are *Sacco a Colleferro*, *Cosa ad Alatri*, and *Sacco a Ceccano* whose altitudes are respectively 218 m, 316 m, and 130 m (Fig. 1). Cosa River is a tributary of Sacco River and streamflow direction is from Colleferro to Ceccano.

2.3. Methods

The workflow of this research is illustrated in Fig. 2. The data analytics methods used in this research are briefly described below. The reader is referred to Ghaderpour and Vujadinovic (2020); Ghaderpour et al. (2018, 2021b, 2024) for more details.

2.3.1. Sequential turning point detection (STPD)

The STPD is briefly described here, similar to a special case of Jumps Upon Spectrum and Trend (JUST) (Ghaderpour and Vujadinovic, 2020; Ghaderpour, 2021). First, the special case of JUST that is only based on linear fit (not seasonal fit) is briefly described below, then STPD is described. Assume that $S_1 = \{y_1, \ldots, y_\tau\}$ and $S_2 = \{y_{\tau+1}, \ldots, y_n\}$ are two segments of a time series of size n, where τ is the potential change point ($1 < \tau < n$). Let

$$y_i = m_1 t_i + b_1 + \varepsilon_i \quad \text{for} \quad 1 \leq i \leq \tau \tag{1}$$

$$y_j = m_2 t_j + b_2 + \varepsilon_j \quad \text{for} \quad \tau < j \leq n \tag{2}$$

where m_1 and m_2 are the gradients, b_1 and b_2 are the intercepts, and ε_i and ε_j are the error terms to be estimated by the Ordinary Least-Squares method (OLS) (Ghaderpour and Vujadinovic, 2020; Ghaderpour et al., 2021a). The JUST algorithm is sensitive to jumps starting at τ, i.e., the estimated pieces can be discontinuous at τ. For example, in environmental monitoring a jump or abrupt change in vegetation index time series might occur due to wildfire or harvesting (Ghaderpour and Vujadinovic, 2020). Though JUST can also detect TPs, the accuracy of the dates of TPs can be less than STPD. In fact, in STPD, it is assumed that there is no jump in the time series at time τ, i.e., the two linear pieces are connected.

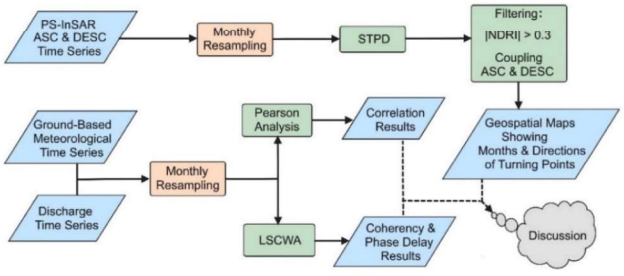

Fig. 2. The workflow of this study. The abbreviations ASC and DESC are for ascending and descending orbits.

Mathematically, in STPD, m_1 and b_1 in equation (1) are first estimated by OLS, then m_1 in equation (2) is only estimated because b_2 is replaced by $\widehat{b}_2 = \widehat{m}_1 t_\tau + \widehat{b}_1$ with $t_j \leftarrow t_j - t_\tau$, $\tau \leq j \leq n$. The potential turning point τ_{forward} $(1 < \tau_{\text{forward}} < n)$ is the one that minimizes the L2 norm of the residual series. The same process is done on the flipped time series to estimate the linear trend with a potential TP, flipped to get τ_{backward} $(1 < \tau_{\text{backward}} < n)$. There is a potential TP if $\text{Diff} = \left|\tau_{\text{forward}} - \tau_{\text{backward}}\right|$ is close enough to zero (e.g., less than 4). If $0 < \text{Diff} < 4$, then the potential TP is the one that has the lowest L2 norm of residuals. The gradient direction or simply direction of the TP is $\widehat{m}_2 - \widehat{m}_1$. If a time series has a TP, then JUST may not accurately detect its date, and accidently estimate a jump due to a high noise level. Likewise, if there is a jump in the time series, then STPD may detect it as a TP with an inaccurate date. Therefore, it is important to define a statistical metric to distinguish jumps from TPs. It is shown that the Normalized Difference Residual Index (NDRI) can do this task effectively, defined as

$$\text{NDRI} = \frac{\|r_2\| - \|r_1\|}{\|r_2\| + \|r_1\|} \tag{3}$$

where $\|\cdot\|$ is the L2 norm, r_1 and r_2 are the residual series of the first and second segments with turning point at τ, respectively. The closer the absolute value of NDRI is to zero, the higher the probability that the detected TP is the true TP. Through an extensive simulation, Ghaderpour et al. (2024) found an effective threshold to distinguish jumps from TPs when applying STPD that is 0.3.

The windowing technique in STPD is the same as the one in JUST. In this technique, a potential TP is estimated for each segment within a moving window that translates or slides over time. Depending on the desired number of CPs or TPs, the window size and step size can be selected by users (Ghaderpour, 2021). Finally, if there are ℓ detected TPs, then a connected linear trend with $\ell + 1$ pieces is fitted to the entire time series to re-estimate the directions of the TPs. Herein, these re-estimated directions are illustrated for the geospatial maps.

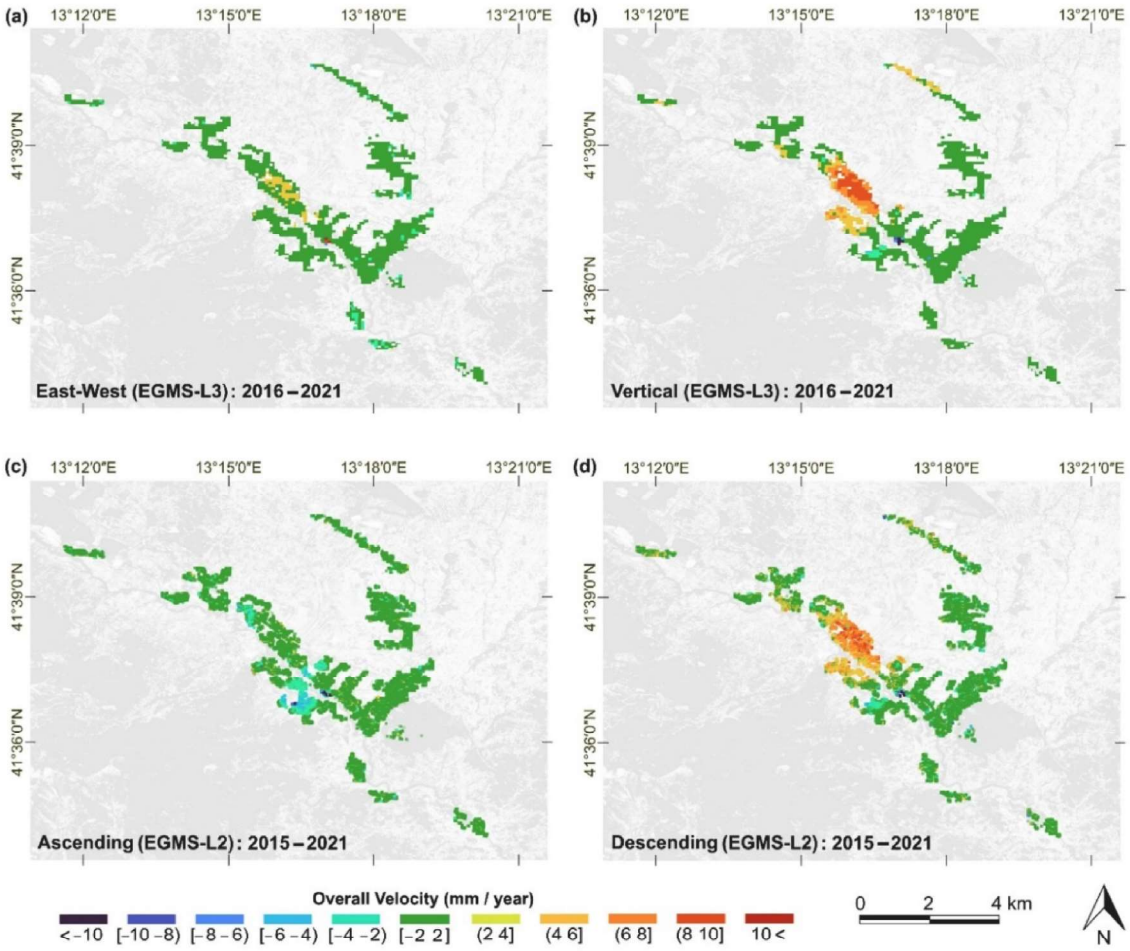

Fig. 3. The maps show the velocities of ground motion for east-west (a), vertical (b), ascending (c), and (d) descending geometries in the industrial zone. Note that the overall velocities shown in panels (a) and (b) are provided by EGMS for the period 2016–2021 while the velocities shown in panels (c) and (d) are estimated by OLS for period 2015–2021. In panel (a), positive (reddish) and negative (bluish) velocities mean eastward and westward motions, respectively. Also, positive (reddish) and negative (bluish) velocities in panels (b), (c), (d) are upward (uplift) and downward (subsidence) motions, respectively (approximately upward and downward for panels (c) and (d) – toward satellite line-of-sight).

2.3.2. Correlation analysis – coefficient of determination

The Pearson's correlation coefficient (r) shows the linear dependency between two variables (e.g., Ratner, 2009; Renaud and Victoria-Feser, 2010). The value range of this coefficient is from −1 to 1. Mathematically, Pearson's method estimates the linear dependency between variables x_i and y_i ($1 \leq i \leq n$) as

$$r = \frac{\sum_{i=1}^{n}(x_i - \overline{x})(y_i - \overline{y})}{\sqrt{\sum_{i=1}^{n}(x_i - \overline{x})^2 \sum_{i=1}^{n}(y_i - \overline{y})^2}} \tag{4}$$

where $\overline{x}$ and $\overline{y}$ are the means of the values of x and y variables, respectively. The value of r^2 or R^2 is called the coefficient of determination, showing the amount of variation in one variable explained by another variable (e.g., Renaud and Victoria-Feser, 2010). This coefficient is used in the present study to identify the strength of linear dependency between normalized precipitation and discharge variables for each station. The R^2 values from 0 to 0.1, from 0.1 to 0.5, and from 0.5 to 1 typically indicate weak, moderate, and strong linear relationships between variables, respectively (e.g., Ratner, 2009).

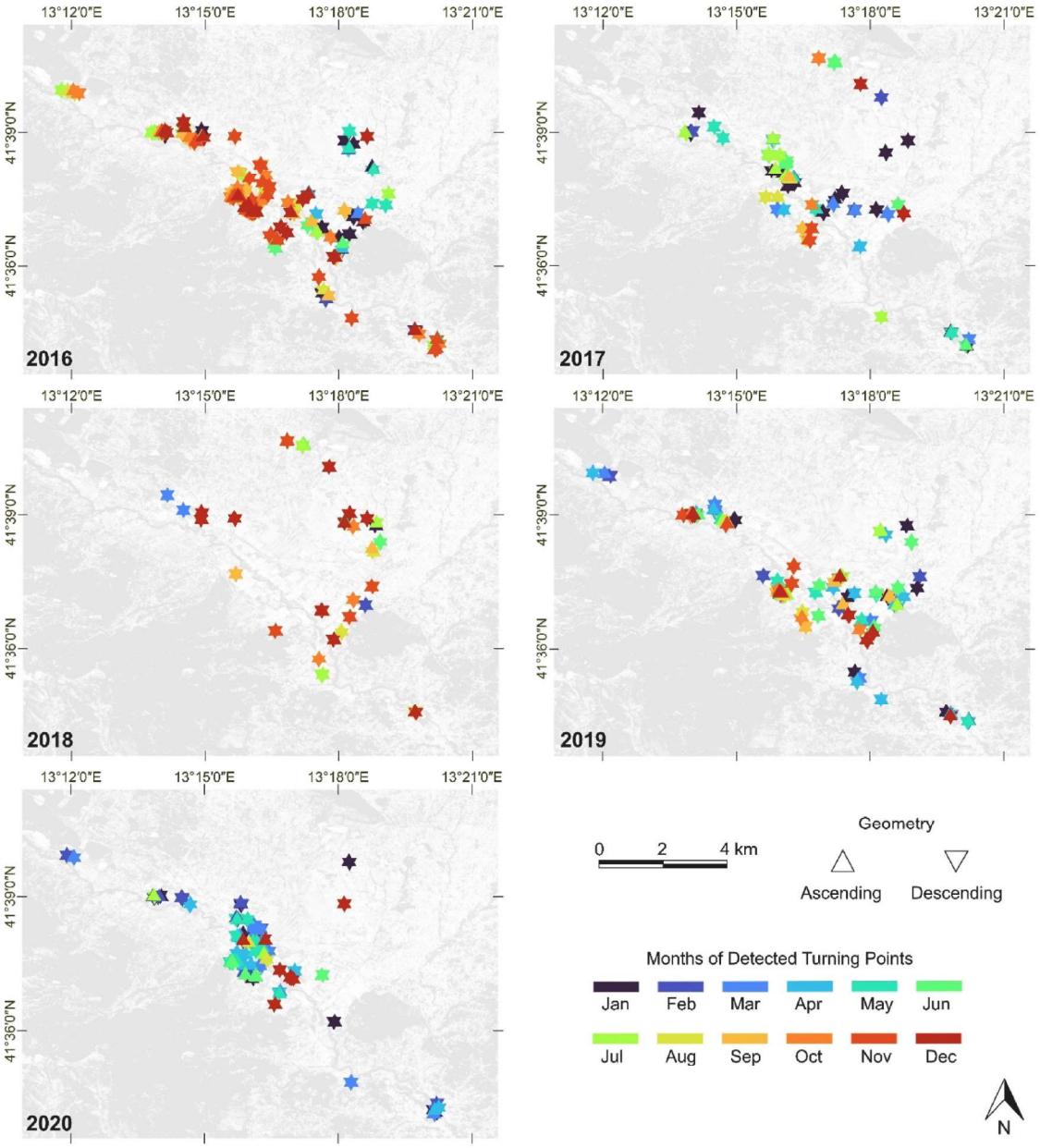

Fig. 4. The geospatial maps show the months of trend turning points in PS-InSAR time series for both ascending and descending orbits. All the estimated TPs are statistically significant at 99% confidence level.

2.3.3. Least-squares cross-wavelet analysis (LSCWA)

The LSCWA is a time-frequency analysis technique that estimates a cross-spectrogram and phase delays between the wavelike components of two time series. Choosing unique sets of frequencies and times, the cross-spectrogram is obtained by entry-wise multiplication of two spectrograms, where each spectrogram is associated with a time series (Ghaderpour et al., 2018, 2021b). A spectrogram is estimated by fitting sinusoids to segments of the time series, where the segment size decreases as frequency increases and vice versa. The percentage variance, displayed on the color bar in a cross-spectrogram, shows how much the wavelike components of the two time series are coherent within a local time-frequency neighborhood: the higher the percentage variance, the higher the coherency. The phase lags/leads, displayed by arrows on the cross-spectrogram, show how much the periodic and aperiodic components in the two time series lag/lead from each other (Ghaderpour et al., 2018, 2021b). The LSCWA is included in the Least-Squares WAVElet software (LSWAVE) (Ghaderpour and Pagiatakis, 2019) and is implemented here (choosing Morlet wavelet) for studying the coherency and phase delay between streamflow and precipitation.

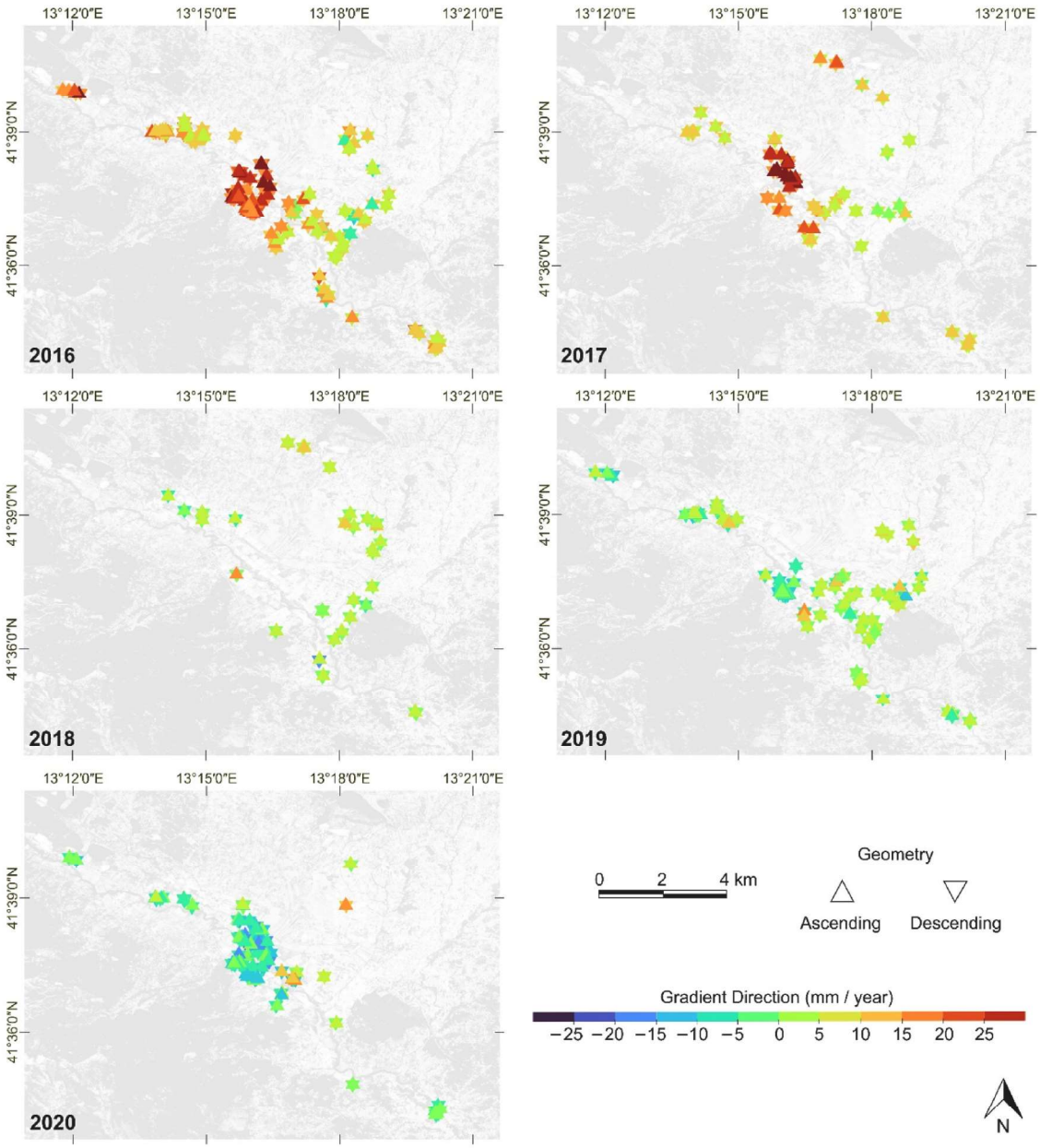

Fig. 5. The geospatial maps show the direction amount of trend turning points in PS-InSAR time series for both ascending and descending orbits.

3. Results

3.1. The PS-InSAR turning point results

To have an idea of the extension of the type of ground movement (e.g., subsidence, uplift, or stable area), especially if it is localized, OLS is applied to all available PS-InSAR time series within the industrial zone, and their overall velocities for entire period 2015–2021 are illustrated in Fig. 3(c) and (d). The estimated velocities of EGMS Ortho products (vertical and east-west directions) are also displayed in Fig. 3(a) and (b) for comparison purposes. Note that year 2015 is not considered for the velocity estimation in Fig. 3(a) and (b) because the Level 3 data for 2015 are not provided by EGMS.

Next, STPD is applied to all the available monthly resampled ascending and descending PS-InSAR time series. The window size and step selected for this analysis are 60 (five years) and 12 (one year), respectively, following the recommendation by Ghaderpour et al. (2024). After the estimation of all the TPs, only the ones with condition $|\text{NDRI}| < 0.3$ are selected to ensure that the detected changes are TPs not jumps, see Ghaderpour et al. (2024). This filtering only removed an insignificant number of TPs for the industrial zone. Since the industrial zone is flat, both ascending and descending acquisitions show approximately the same increasing/decreasing trend pattern. Therefore, to further increase the reliability of the detected TPs, only ascending and descending PSs are selected that have the same TPs and are within 50 m apart from each other. After the filtering, 317 ascending and 298 descending time series remain, where each time series has two TPs. The geospatial maps of the TPs and their corresponding gradient directions for these time series are illustrated in Figs. 4 and 5, respectively. The STPD is set to not estimate any TPs in the years 2015 and 2022 due to potential seasonal noise. Therefore, the geospatial maps only show TPs for the years 2016–2021. Two examples of these time series are shown in Fig. 6, where |NDRI| and DIR (direction) are written in red, and the overall velocities are written in black. These velocities are illustrated in Fig. 3. It can be seen from Fig. 3 that in areas near the coordinates 41°38″ N and 13°16″ E, most of descending PS-InSAR time series show a positive overall velocity. From Figs. 5 and 6, the displacement time series has a negative gradient before the TPs in 2016 and 2017, where the directions of TPs become positive. During 2018, the displacement has a positive gradient until 2019 and 2020, where

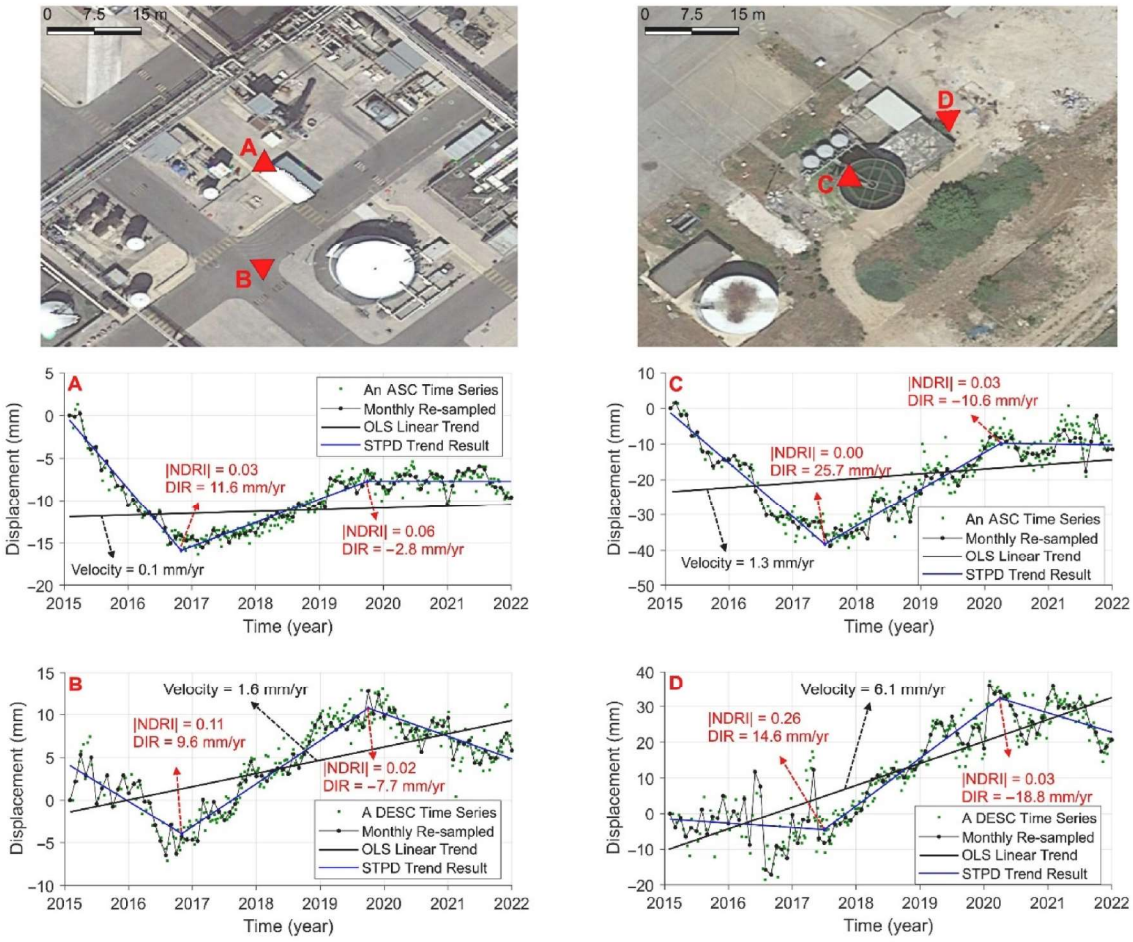

Fig. 6. Two examples of coupled ascending and descending PS-InSAR having the same turning points.

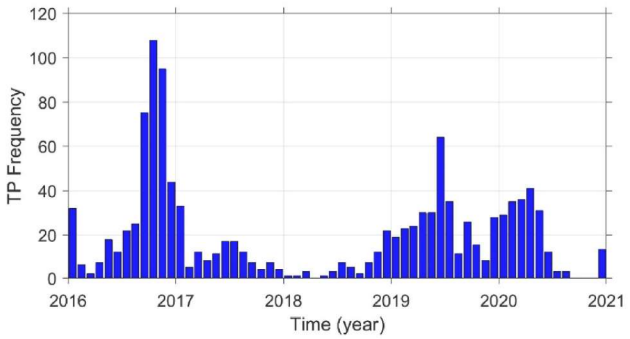

Fig. 7. The number of TPs detected for each calendar month during 2016–2020.

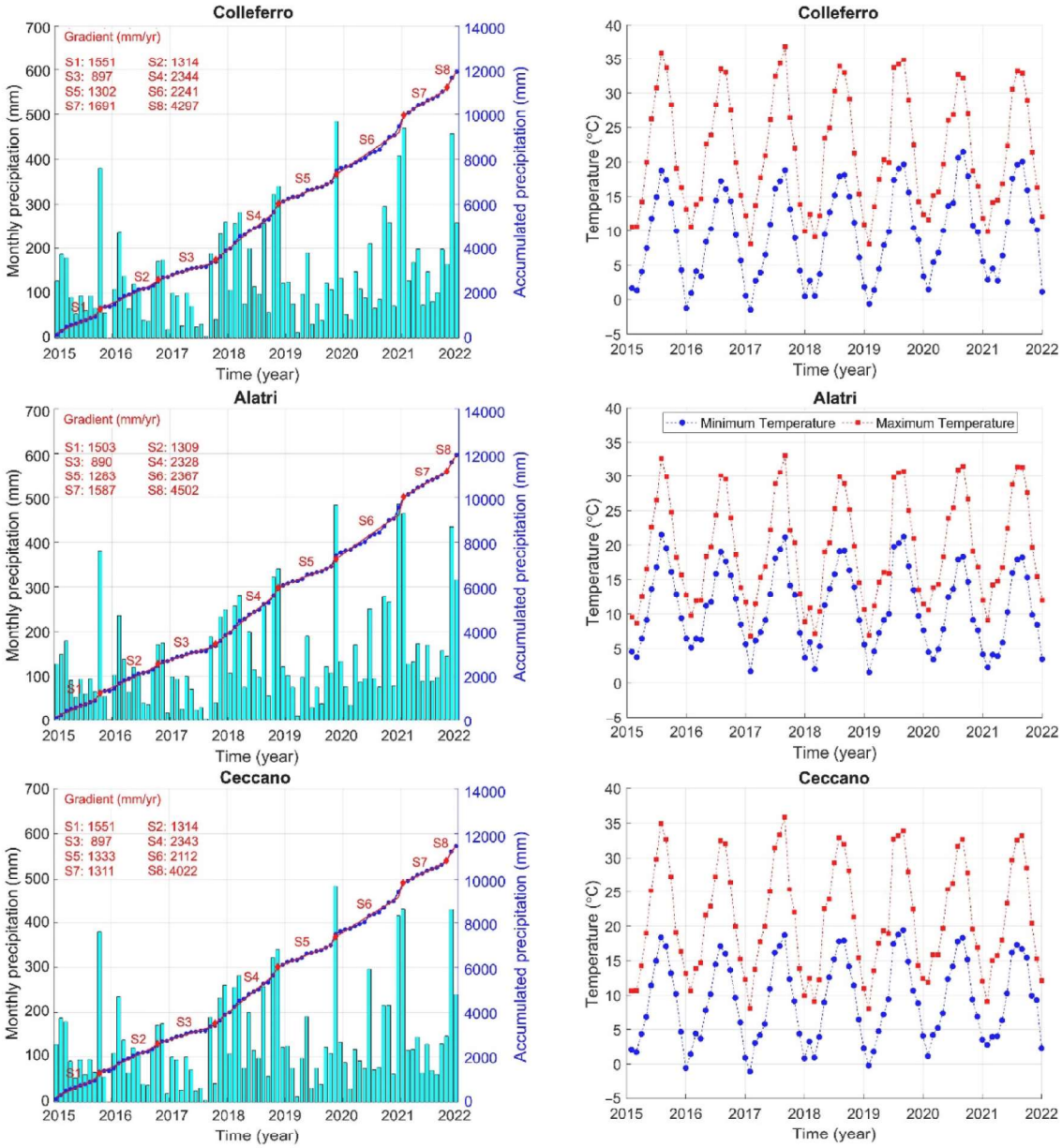

Fig. 8. The monthly meteorological time series for Colleferro, Alatri, and Ceccano.

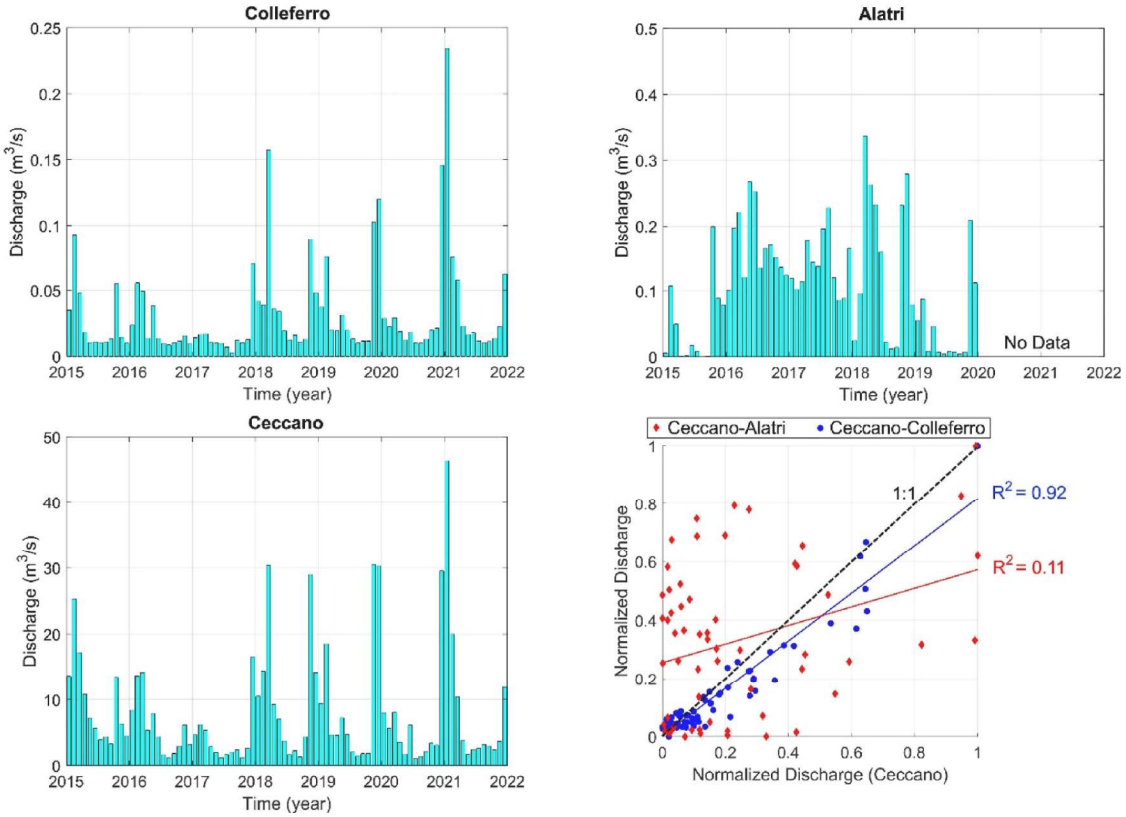

Fig. 9. The discharge time series for Colleferro, Alatri, and Ceccano and their coefficients of determination.

the directions of TPs become negative. To better visualize the temporal distribution of TPs, the frequency bar charts of the TPs illustrated in Fig. 4 are displayed in Fig. 7. One can see that not many TPs are estimated in 2018. The displacement time series have a positive gradient (velocity) during 2018 for the entire industrial zone, indicating land uplift.

3.2. *The meteorological and streamflow results*

Monthly precipitation, maximum and minimum temperature time series for towns of Colleferro, Alatri, and Ceccano are illustrated in Fig. 8. The temperature in 2017 was significantly higher than the temperature in 2018. For example, the maximum temperature was 36 °C in August of 2017 while it reduced to 32 °C in August of 2018 for Ceccano. The special case of JUST as modeled by equations (1) and (2) was applied to the accumulated precipitation time series to detect CPs using a three-year-long moving window. The JUST estimated trend is also illustrated in Fig. 8. Comparing the gradients of the linear pieces in 2017 and 2018 (S3 and S4), one can see that the gradient of accumulated precipitation increased more than 2.5 times. Monthly streamflow (discharge) time series for the three hydrometric stations shown in Fig. 1 are illustrated in Fig. 9. The amount of discharge recorded at stations *Sacco a Ceccano* is much higher at stations *Sacco a Colleferro* and *Cosa ad Alatri* due to factors, such as tributaries, characteristics of drainage basins, and man-made surfaces. Herein, the relative discharge is more important at each station as it shows the influence of anthropogenic activities and climate change. The coefficient of determination between Colleferro and Ceccano is $R^2 = 0.92$ while a much lower coefficient is observed between Alatri and Ceccano ($R^2 = 0.11$). This may be explained by the fact that Cosa River is a tributary of Sacco River and has its own hydrological characteristics, and it travels through the town of Frosinone.

The cross-spectrograms of the monthly discharge and precipitation time series are displayed in Fig. 10. Panel (a) clearly shows that the periodic and aperiodic components of discharge time series are in-phase. There are statistically significant seasonal peaks in 2018 and 2019 (4 cycles/year or three-month period) as shown in Fig. 10(a). The wavelike components of discharge time series for Alatri and Ceccano are less significant as can be seen from panel (b). Panels (c) and (e) show a phase lag of about 30° for annual and seasonal cycles of streamflow and precipitation. In other words, the annual cycle of precipitation generally leads the one in the discharge time series by about one month. Similarly, the seasonal cycles of precipitation lead the ones in the discharge time series. Interestingly, there is no statistically significant coherency between the discharge and precipitation time series for Colleferro and Ceccano in 2017 while in 2018 there are statistically significant seasonal cycles in precipitation and discharge time series, significantly coherent with a time delay, see Fig. 10(c) and (e). This shows a clear interaction between climate and streamflow. The coefficients of determination (R^2)

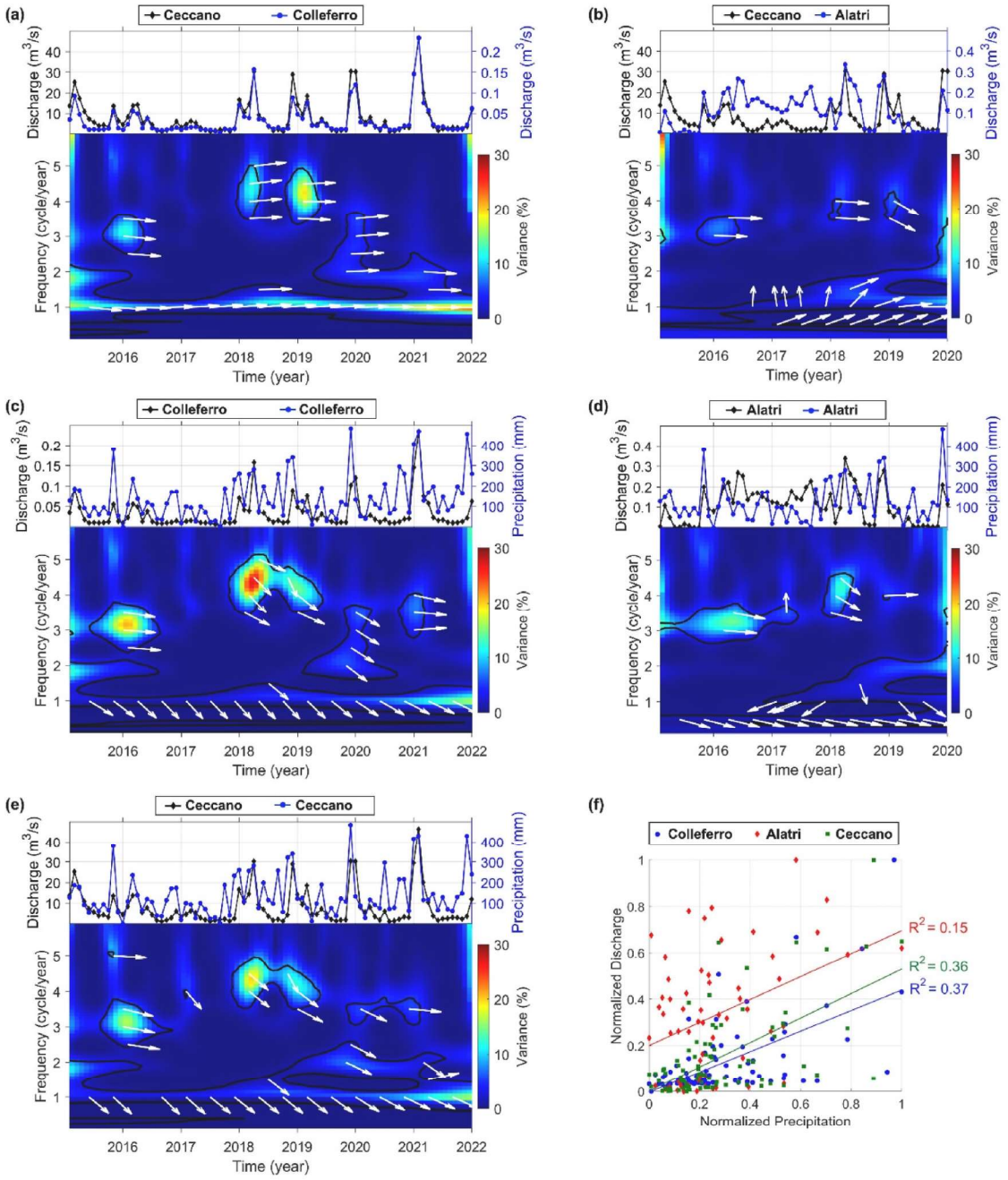

Fig. 10. The monthly precipitation and streamflow time series and their LSCWA and coefficients of determination. The peaks inside the black contour lines are statistically significant at 95% confidence level. The white arrows show the phase delays that are displayed on the most significant coherent peaks. The arrows pointing to the east and west mean in-phase and out-of-phase. The arrows pointing toward north and south mean the cycles of the time series in black leads and lags from the ones in blue, respectively. (For interpretation of the references to color in this figure legend, the reader is referred to the Web version of this article.)

between precipitation and streamflow are also shown in Fig. 10(f), but they do not show how the components of the time series are correlated at different periods, highlighting the advantages of using LSCWA.

4. Discussion

An advantage of STPD over traditional regression models is the ability to estimate the dates when the displacement trends have changed their directions. For example, Fig. 3(d) shows that many PS-InSAR time series have an increasing trend during 2015–2021 with a velocity between 4 and 8 mm/year near 41°38″ N and 13°16″ E. On the other hand, Figs. 4 and 6 show that these time series have a negative velocity during 2015 and 2016 which turns to positive after late 2016. While the same behavior is observed in the ascending time series (e.g., see time series A and C in Fig. 6), their overall trends remain insignificant, displayed in green in Fig. 3(c). Moreover, the velocities toward the vertical direction, shown in Fig. 3(b), near 41°38″ N and 13°16″ E are positive, indicating land uplift.

The selection of five-year-long moving window in STPD allowed robust detection of slow-moving ground deformation and was less sensitive to seasonal noise. In other words, smaller window sizes could potentially increase the false positive rate, e.g., turning points may be near the minimum or maximum values of seasonal or annual cycles observed in PS-InSAR time series. Coupling the PS-InSAR time series of ascending and descending orbits increased the reliability of the estimated TPs, though this filtering reduced the spatial coverage of the PSs. A random set of PS-InSAR time series were also selected and their estimated TPs were visually inspected to ensure their accuracy. The STPD results showed mainly two TPs for each PS-InSAR time series, where the first one with a positive direction was in 2016 or 2017 and the second one with a negative direction was in 2019 or 2020. This indicated land subsidence prior to 2018 followed by land uplift during 2018.

This study has some limitations. Unfortunately, there was no information available on groundwater level to conduct a more rigorous statistical analysis. In addition, no information was available for water extraction amount by the industrial settlements in the study region. However, climate and surface streamflow are highly correlated with groundwater (Jiang et al., 2022; Saha et al., 2017). Relatively higher temperature and lower precipitation and streamflow in 2016 and 2017 (the drier period) as well as water pumping likely reduced the groundwater level, resulting in land subsidence as observed in PS-InSAR time series. On the other hand, relatively lower temperature and higher precipitation and streamflow in 2018 (the wetter period) as well as reduction of pumping water likely increased the groundwater level, resulted in significant land uplift during 2018 as observed by Sentinel-1 satellites. These results also agree with the results presented by Allocca et al. (2015) who demonstrated how an increased amount of precipitation has a significant impact on groundwater recharge in the central-southern part of the Terminio Mount karst aquifer in Campania region, Italy. The use of PS-InSAR and STPD techniques for detecting changes in ground motion velocity as presented herein may also help hydrogeologists in estimating and/or calibrating groundwater level (Allocca et al., 2014, 2015).

5. Conclusions

In this study, ground deformation for an industrial zone in Sacco River Valley in Central Italy was studied though processing PS-InSAR time series by STPD. The correlation between the detected displacement TPs and ground-based measurements were also investigated. The direction of the estimated TPs in the PS-InSAR time series agreed with the change in gradients of precipitation and streamflow fluctuation. The LSCWA showed that the seasonal cycles of precipitation and streamflow time series were significantly coherent with time delay of few weeks in 2018 while no significant peaks were observed in 2017. The significant increase in the accumulated precipitation in 2018 and relatively lower temperature have increased the discharge of the river and potentially recharged groundwater which can explain the land uplift during 2018 in the industrial zone. The results of this study may be useful for geologists, hydrologists, and other scientists as well as stakeholders and responsible authorities for building a sustainable environment and reduce the potential risks to infrastructures and public health.

Funding

This study was carried out within the Spoke VS2 Ground Instabilities of the RETURN Extended Partnership and received funding from the European Union Next-GenerationEU (National Recovery and Resilience Plan – NRRP, Mission 4, Component 2, Investment 1.3 – D.D. 1243 August 2, 2022, PE0000005).

Software

The STPD and LSCWA code implemented in this research are freely available at: https://github.com/Ghaderpour/LSWAVE-SignalProcessing.

Ethical Statement for Solid State Ionics

Hereby, I, Ebrahim Ghaderpour consciously assure that for the manuscript “Ground Deformation Monitoring via PS-InSAR Time Series: An Industrial Zone in Sacco River Valley, Central Italy” the following is fulfilled.

1) This material is the authors’ own original work, which has not been previously published elsewhere.
2) The paper is not currently being considered for publication elsewhere.
3) The paper reflects the authors’ own research and analysis in a truthful and complete manner.
4) The paper properly credits the meaningful contributions of co-authors and co-researchers.
5) The results are appropriately placed in the context of prior and existing research.
6) All sources used are properly disclosed (correct citation). Literally copying of text must be indicated as such by using quotation marks and giving proper reference.
7) All authors have been personally and actively involved in substantial work leading to the paper, and will take public responsibility for its content.

The violation of the Ethical Statement rules may result in severe consequences.

To verify originality, your article may be checked by the originality detection software iThenticate. See also http://www.elsevier.com/editors/plagdetect.

I agree with the above statements and declare that this submission follows the policies of Solid State Ionics as outlined in the Guide for Authors and in the Ethical Statement.

CRediT authorship contribution statement

Ebrahim Ghaderpour: Writing – original draft, Visualization, Validation, Software, Methodology, Formal analysis, Data curation, Conceptualization. **Paolo Mazzanti:** Writing – review & editing, Conceptualization. **Francesca Bozzano:** Writing – review & editing, Conceptualization. **Gabriele Scarascia Mugnozza:** Writing – review & editing, Conceptualization.

Declaration of competing interest

The authors declare that they have no known competing financial interests or personal relationships that could have appeared to influence the work reported in this paper.

Data availability

Data will be made available on request.

Acknowledgments

The authors thank European Ground Motion Service personnel for providing the PS-InSAR datasets used in this research. The authors also thank Regione Lazio – Agenzia Regionale di Protezione Civile - Prevenzione, Pianificazione e Previsione Centro Funzionale Regionale for providing the discharge time series.

References

Allocca, V., Coda, S., Calcaterra, D., De Vita, P., 2022. Groundwater rebound and flooding in the Naples' periurban area (Italy). J. Flood Risk Manag. 15, e12775.
Allocca, V., De Vita, P., Manna, F., Nimmo, J.R., 2015. Groundwater recharge assessment at local and episodic scale in a soil mantled perched karst aquifer in southern Italy. J. Hydrol. 529, 843–853.
Allocca, V., Manna, F., De Vita, P., 2014. Estimating annual groundwater recharge coefficient for karst aquifers of the southern Apennines (Italy). Hydrol. Earth Syst. Sci. 18, 803–817.
Awty-Carroll, K., Bunting, P., Hardy, A., Bell, G., 2019. An evaluation and comparison of four dense time series change detection methods using simulated data. Rem. Sens. 11, 2779.
Bai, L., Jiang, L., Wang, H., Sun, Q., 2016. Spatiotemporal characterization of land subsidence and uplift (2009–2010) over Wuhan in Central China revealed by TerraSAR-X InSAR analysis. Rem. Sens. 8, 350.
Beccaro, L., Cianflone, G., Tolomei, C., 2019. Insar-based detection of subsidence affecting infrastructures and urban areas in Emilia-Romagna Region (Italy). J. Hydrol. 569, 470–482.
Bozzano, F., Esposito, C., Franchi, S., Mazzanti, P., Perissin, D., Rocca, A., Romano, E., 2015. Influence of underground structures and infrastructures on the groundwater level in the urban area of Milan, Italy. Remote Sens. Environ. 168, 219–238.
Calò, F., Ardizzone, F., Castaldo, R., Lollino, P., Tizzani, P., Guzzetti, F., Lanari, R., Angeli, M.G., Pontoni, F., Manunta, M., 2014. Enhanced landslide investigations through advanced DInSAR techniques: the Ivancich case study, Assisi, Italy. Remote Sens. Environ. 142, 69–82.
Chen, B., Gong, H., Chen, Y., Li, X., Zhou, C., Lei, K., Zhu, L., Duan, L., Zhao, X., 2020. Land subsidence and its relation with groundwater aquifers in Beijing Plain of China. Sci. Total Environ. 735, 139111.
Coda, S., Confuorto, P., De Vita, P., Di Martire, D., Allocca, V., 2019a. Uplift evidences related to the recession of groundwater abstraction in a Pyroclastic-Alluvial Aquifer of Southern Italy. Geosciences 9, 215.
Coda, S., Tessitore, S., Di Martire, D., Calcaterra, D., De Vita, P., Allocca, V., 2019b. Coupled ground uplift and groundwater rebound in the metropolitan city of Naples (southern Italy). J. Hydrol. 569, 470–482.
Colombo, L., Gattinoni, P., Scesi, L., 2017. Influence of underground structures and infrastructures on the groundwater level in the urban area of Milan, Italy. Int. J. Sustain. Dev. Plann. 12, 176–184.
Crosetto, M., Monserrat, O., Cuevas-González, M., Devanthéry, N., Crippa, B., 2016. Persistent scatterer interferometry: a review. ISPRS J. Photogrammetry Remote Sens. 115, 78–89.
Festa, D., Bonano, M., Casagli, N., Confuorto, P., De Luca, C., Del Soldato, M., Lanari, R., Lu, P., Manunta, M., Manzo, M., Onorato, G., Raspini, F., Zinno, I., Casu, F., 2022. Nation-wide mapping and classification of ground deformation phenomena through the spatial clustering of P-SBAS InSAR measurements: Italy case study. ISPRS J. Photogrammetry Remote Sens. 189, 1–22.
Fu, G., Schmid, W., Castellazzi, P., 2023. Understanding the spatial variability of the relationship between InSAR-derived deformation and groundwater level using machine learning. Geosciences 13, 133.
Ghaderpour, E., 2021. JUST: MATLAB and Python software for change detection and time series analysis. GPS Solut. 25, 85.
Ghaderpour, E., Antonielli, B., Bozzano, F., Scarascia Mugnozza, G., Mazzanti, P., 2024. A fast and robust method for detecting trend turning points in PS-InSAR displacement time series. Comput. Geosci. 185, 105546.
Ghaderpour, E., Ince, E., Pagiatakis, S., 2018. Least-squares cross-wavelet analysis and its applications in geophysical time series. J. Geodyn. 92, 1223–1236.
Ghaderpour, E., Pagiatakis, S., 2019. LSWAVE: a MATLAB software for the least-squares wavelet and cross wavelet analyses. GPS Solut. 23, 50.
Ghaderpour, E., Pagiatakis, S.D., Hassan, Q.K., 2021a. A survey on change detection and time series analysis with applications. Appl. Sci. 11, 6141.
Ghaderpour, E., Vujadinovic, T., 2020. Change detection within remotely-sensed satellite image time series via spectral analysis. Rem. Sens. 12, 4001.
Ghaderpour, E., Vujadinovic, T., Hassan, Q., 2021b. Application of the least-squares wavelet software in hydrology: athabasca River Basin. J. Hydrol. Reg. Stud. 36C, 100847.
Hu, X., Lu, Z., Pierson, T.C., Kramer, R., George, D.L., 2018. Combining InSAR and GPS to determine transient movement and thickness of a seasonally active low-gradient translational landslide. Geophys. Res. Lett. 45, 1453–1462.
Hussain, M.A., Chen, Z., Zheng, Y., Shoaib, M., Ma, J., Ahmad, I., Asghar, A., Khan, J., 2022. PS-InSAR based monitoring of land subsidence by groundwater extraction for Lahore Metropolitan City, Pakistan. Rem. Sens. 14, 3950.
Jasechko, S., Seybold, H., Perrone, D., Fan, Y., Shamsudduha, M., Taylor, R.G., Fallatah, O., Kirchner, J.W., 2024. Rapid groundwater decline and some cases of recovery in aquifers globally. Nature 625, 715–721.
Jiang, X., Ma, R., Ma, T., Sun, Z., 2022. Modeling the effects of water diversion projects on surface water and groundwater interactions in the central Yangtze River basin. Sci. Total Environ. 830, 154606.
Li, J., Li, Z.-L., Wu, H., You, N., 2022. Trend, seasonality, and abrupt change detection method for land surface temperature time-series analysis: evaluation and improvement. Remote Sens. Environ. 280, 113222.
Li, H., Zhu, L., Guo, G., Zhang, Y., Dai, Z., Li, X., Chang, L., Teatini, P., 2021. Land subsidence due to groundwater pumping: hazard probability assessment through the combination of bayesian model and fuzzy set theory. Nat. Hazards Earth Syst. Sci. 21, 823–835.

Massimo, A., Dell'Isola, M., Frattolillo, A., Ficco, G., 2014. Development of a geographical information system (GIS) for the integration of solar energy in the energy planning of a wide area. Sustainability 6, 5730–5744.
Mateos, R.M., Ezquerro, P., Luque-Espinar, J.A., Béjar-Pizarro, M., Notti, D., Azañón, J.M., Montserrat, O., Herrera, G., Fernández-Chacón, F., Peinado, T., 2017. Multiband PSInSAR and long-period monitoring of land subsidence in a strategic detrital aquifer (Vega de Granada, SE Spain): an approach to support management decisions. J. Hydrol. 553, 71–87.
Mazzanti, P., Bozzano, F., Cipriani, I., Prestininzi, A., 2015. New insights into the temporal prediction of landslides by a terrestrial SAR interferometry monitoring case study. Landslides 12, 55–68.
Moretto, S., Bozzano, F., Mazzanti, P., 2021. The role of satellite InSAR for landslide forecasting: limitations and openings. Rem. Sens. 13, 3735.
Notti, D., Herrera, G., Bianchini, S., Meisina, C., García-Davalillo, J.C., Zucca, F., 2014. A methodology for improving landslide PSI data analysis. Int. J. Rem. Sens. 35, 2186–2214.
Perrone, P., Lettieri, G., Marinaro, C., Longo, V., Capone, S., Forleo, A., Pappalardo, S., Montano, L., Piscopo, M., 2022. Molecular alterations and severe abnormalities in spermatozoa of young men living in the "valley of Sacco River" (latium, Italy): a preliminary study. Int. J. Environ. Res. Publ. Health 19, 11023.
Ratner, B., 2009. The correlation coefficient: its values range between +1/−1, or do they? J. Target Meas. Anal. Market. 17, 139–142.
Renaud, O., Victoria-Feser, M.-P., 2010. A robust coefficient of determination for regression. J. Stat. Plann. Inference 140, 1852–1862.
Ren, T., Gong, W., Gao, L., Zhao, F., Cheng, Z., 2022. An interpretation approach of ascending–descending SAR data for landslide identification. Rem. Sens. 14, 1299.
Rocca, A., Mazzanti, P., Perrisin, D., Bozzano, F., 2014. Detection of past slope activity in a desert area using multi-temporal DInSAR with alos palsar data. Ital. J. Eng. Geol. Environ. 1, 35–49.
Rosen, P., Hensley, S., Joughin, I., Li, F., Madsen, S., Rodriguez, E., Goldstein, R., 2000. Synthetic aperture radar interferometry. Proc. IEEE 88, 333–382.
Saha, G., Li, J., Thring, R., Hirshfield, F., Paul, S., 2017. Temporal dynamics of groundwater-surface water interaction under the effects of climate change: a case study in the Kiskatinaw River basin, Canada. J. Hydrol. 551, 440–452.
Saroli, M., Albano, M., Modoni, G., Moro, M., Milana, G., Spacagna, R.-L., Falcucci, E., Gori, S., Scarascia Mugnozza, G., 2020. Insights into bedrock paleomorphology and linear dynamic soil properties of the Cassino intermontane basin (Central Italy). Eng. Geol. 264, 105333.
Saroli, M., Lancia, M., Petitta, M., 2019. The geology and hydrogeology of the Cassino plain (central Apennines, Italy): redefining the regional groundwater balance. Hydrogeol. J. 27, 1563–1579.
Sousa, J.J., Ruiz, A.M., Hanssen, R.F., Bastos, L., Gil, A.J., Galindo-Zaldívar, J., de Galdeano, C.S., 2010. PS-InSAR processing methodologies in the detection of field surface deformation–study of the Granada basin (Central Betic Cordilleras, southern Spain). J. Geodyn. 49, 181–189.
Tang, W., Zhao, X., Motagh, M., Bi, G., Li, J., Chen, M., Chen, H., Liao, M., 2022. Land subsidence and rebound in the Taiyuan basin, northern China, in the context of inter-basin water transfer and groundwater management. Remote Sens. Environ. 269, 112792.
Tarquini, S., Isola, I., Favalli, M., Battistini, A., Dotta, G., 2023. TINITALY, a Digital Elevation Model of Italy with a 10 Meters Cell Size. version 1.1. Istituto Nazionale di Geofisica e Vulcanologia (INGV).
Tarquini, S., Nannipieri, L., 2017. The 10 m-resolution TINITALY DEM as a trans-disciplinary basis for the analysis of the Italian territory: current trends and new perspectives. Geomorphology 281, 108–115.
Teatini, P., Ferronato, M., Gambolati, G., Bertoni, W., Gonella, M., 2005. A century of land subsidence in Ravenna, Italy. Environ. Geol. 47, 831–846.
Wang, H., Jiao, Y., Hu, B., Li, F., Li, D., 2023. Study on interaction between surface water and groundwater in typical reach of Xiaoqing River based on WEP-L model. Water 15, 492.
Wu, W., Lo, M., Wada, Y., Famiglietti, J., Reager, J., Yeh, P.J.F., Ducharne, A., Yang, Z., 2020. Divergent effects of climate change on future groundwater availability in key mid-latitude aquifers. Nat. Commun. 11, 3710.
Yao, J., Yao, X., Liu, X., 2022. Landslide detection and mapping based on SBAS-InSAR and PS-InSAR: a case study in Gongjue County, Tibet, China. Rem. Sens. 14, 4728.
Zaghloul, M.S., Ghaderpour, E., Dastour, H., Farjad, B., Gupta, A., Eum, H., Achari, G., Hassan, Q.K., 2022. Long term trend analysis of river flow and climate in Northern Canada. Hydrology 9, 197.
Zhang, L., Ding, X., Lu, Z., 2011. Modeling PSInSAR time series without phase unwrapping. IEEE Transctions Geosci. Rem. Sens. 49, 547–556.